

DRAFT VERSION DECEMBER 16, 2021

Typeset using L^AT_EX preprint style in AASTeX63

STELLAR PARAMETRIZATION OF LAMOST M DWARF STARS

JIADONG LI ^{1,2} CHAO LIU ^{1,2} BO ZHANG ³ HAO TIAN ¹ DAN QIU,^{4,5} AND HAIJUN TIAN^{4,5}

¹*Key Laboratory of Space Astronomy and Technology, National Astronomical Observatories, CAS,
Beijing 100101, China*

²*University of Chinese Academy of Sciences,
Beijing 100049, China*

³*Department of Astronomy, Beijing Normal University,
Beijing 100875, China*

⁴*China Three Gorges University,
Yichang 443002, China*

⁵*Center of Astronomy and Space Science Research, China Three Gorges University,
Yichang 443002, China*

(Revised January 29, 2021; Accepted January 30, 2021)

ABSTRACT

M dwarf stars are the most common stars in the Galaxy, dominating the population of the Galaxy by numbers at faint magnitudes. Precise and accurate stellar parameters for M dwarfs are of crucial importance for many studies. However, the atmospheric parameters of M dwarf stars are difficult to be determined. In this paper, we present a catalog of the spectroscopic stellar parameters (T_{eff} and $[M/H]$) of $\sim 300,000$ M dwarf stars observed by both LAMOST and *Gaia* using Stellar Label Machine (SLAM). We train a SLAM model using LAMOST spectra with APOGEE Data Release 16 (DR16) labels with $2800 < T_{eff} < 4500\text{K}$ and $-2 < [M/H] < 0.5$ dex. The SLAM T_{eff} is in agreement to within $\sim 50\text{K}$ compared to the previous study determined by APOGEE observation, and SLAM $[M/H]$ agree within 0.12 dex compared to the APOGEE observation. We also set up a SLAM model trained by BT-Settl atmospheric model, with random uncertainties (in cross-validation) to 60K and agree within $\sim 90\text{K}$ compared to previous study.

Keywords: methods: data analysis — stars: low mass — stars: fundamental parameters — stars: late-type — survey

1. INTRODUCTION

In the Galaxy, M dwarfs are inherently faint objects, but dominate the faint magnitudes of the Galaxy by numbers, making up $\sim 70\%$ in our Galaxy (Bochanski et al. 2010). Kirkpatrick et al. (1999) discovered spectral classes *L* and *T* using the Two Micron All Sky Survey (2MASS; Skrutskie

et al. 2006). T type stars are completely comprised of brown dwarfs, while main-sequence (MS) stars earlier than M type are comprised of hydrogen-burning. M dwarf stars, which are at the MS end of the Hertzsprung-Russell (H-R) diagram, are in between the former and the later and show admixture features of both.

The M dwarf stars have lifetimes much longer than the Hubble time (Bochanski et al. 2010), which makes them valuable for tracing the chemical and dynamical history of the Galaxy. Previous studies also used M dwarf stars to determine the initial mass function (IMF) (Covey et al. 2008; Bochanski et al. 2010) at low-mass end. Furthermore, M dwarfs are primary candidates for exoplanet searching (Trifonov et al. 2018). Accurate and precise parameters including effective temperatures and chemical compositions of the planet-host stars play a key role in looking for habitable exoplanets.

The M dwarf stars are classified at wavelengths 6300 to 9000 Å (Boeshaar 1976; Kirkpatrick 1992; Boeshaar & Tyson 1985). One of the main difficulties is that the prominent molecular absorption in the spectra of M dwarfs, are hard to predict by atmospheric models (Mann et al. 2015). Moreover, obtaining spectra with high quality for these faint objects is challenging. Generally, the measurement of equivalent widths (EWs) and synthesis are the classical and most common methods to derive stellar parameters. However, synthesis is the favorable method to measure the stellar parameters for cool stars since the EWs are difficult to be measured for their crowded absorption lines (reviewed by Jofré et al. 2019).

With the development of new facilities, large surveys such as the Sloan Digital Sky Survey, Apache Point Observatory Galactic Evolution Experiment (SDSS/APOGEE; Majewski et al. 2017), Transiting Exoplanet Survey Satellite (Muirhead et al. 2018) (*TESS*) missions and the Large Sky Area Multi-Object Fiber Spectroscopic Telescope (LAMOST; Cui et al. 2012; Deng et al. 2012; Zhao et al. 2012) make incremental photometric and spectroscopic data of M dwarf stars. The LAMOST survey has provided nine million spectra in its Data Release 6 (DR6) at $R \sim 1800$, among which $\sim 600,000$ spectra are M dwarf stars. However, these stars are lack of stellar parameters.

Many efforts have attempted to decode the effective temperatures and chemical abundances of M dwarfs from high-resolution spectra either in the optical or near-infrared (NIR) band (Woolf & Wallerstein 2005; Rajpurohit et al. 2014, 2018; Veyette et al. 2017; Mann et al. 2019). The APOGEE Stellar Parameter and Chemical Abundances Pipeline (ASPCAP) measurements of T_{eff} and metallicity (García Pérez et al. 2016) for M dwarfs have been determined with precisions of ~ 100 K and 0.18 dex, respectively (Schmidt et al. 2016) by fitting with the atmospheric models. Furthermore, the APOGEE data of SDSS Data Release 16 (DR16) (Jönsson et al. 2020) use new atmospheric grids which can estimate effective temperatures down to 3000K. Birky et al. (2020, hereafter B20) using *The Cannon* (Ness et al. 2015; Ho et al. 2017) derived the effective temperature and metallicities for 5,875 APOGEE M dwarfs with 87 sources from Mann et al. (2015, hereafter M15) as training dataset. M15 estimated effective temperatures by comparing spectra with the BT-Settl atmospheric models (Allard et al. 2013) and calibrated their results using stars with determinations from interferometry (Boyajian et al. 2012; Mann et al. 2013).

Furthermore, Rajpurohit et al. (2018) determined parameters of 45 M dwarfs using high-resolution H-band spectra by fitting BT-Settl model grids. Dieterich et al. (2020) obtained stellar parameters of five M dwarf systems by fitting BT-Settl atmospheric and test current stellar models. Galgano et al. (2020) presented effective temperatures, radii, masses, and luminosities for 29,678 M dwarfs from LAMOST DR1 using *The Cannon* with a typical uncertainty of T_{eff} of ~ 110 K. They used stellar

labels from *TESS* Cool Dwarf Catalog (Muirhead et al. 2018), in which T_{eff} was determined from the color- T_{eff} relations in M15. In other words, the effective temperatures of all previous studies rely on the BT-Settl atmospheric model. It is noted that the parameters derived by the previous works display substantial systematic errors, since different works used the different spectral regions and lines with various methods (Jofré et al. 2019).

Recently, new techniques to derive stellar parameters with machine learning algorithms (Ting et al. 2019; Xiang et al. 2019) have become efficient for large data of spectra survey. Data-driven methods were illustrated as promising solutions in cool star parameterization (Jofré et al. 2019). These novel methods have well performed in transferring the known information from training datasets to entire datasets.

In this work, we build a data-driven model for LAMOST spectra based on Stellar Label Machine (SLAM; Zhang et al. 2020) trained by APOGEE stellar labels and BT-Settl model atmospheres and synthetic spectra (Allard et al. 2013) to estimate the entire dataset of LAMOST M dwarf stars.

This paper is organized as follows. In section 2, we introduce how SLAM works. In section 3, we describe M dwarf spectra selected from the LAMOST and *Gaia* surveys as well as the training dataset from APOGEE survey and BT-Settl model. We then present the results in section 4 and make comparison with previous works. Section 5 raises discussions about the caveats of the results, and we assess the robustness and performance of the results and draw conclusions in section 5.

2. METHOD

Stellar Label Machine (SLAM), developed by Zhang et al. (2020), has shown good performance in determining the stellar labels of LAMOST DR5. It is a data-driven model based on Support Vector Regression (SVR) (Vapnik et al. 1997), which is a robust non-linear regression model. The data-driven method has been demonstrated as one of the most practical ways to measure the stellar parameters of M dwarfs. Additionally, LAMOST data is suitable for data-driven methods because the spectra of low resolution are hard to perform the standard methods of measuring EWs for parameters estimations of cool stars (Jofré et al. 2019). Meanwhile, the large quantity of LAMOST dataset demands to conduct fast data-driven methods.

2.1. Support Vector Regression

Support-vector machine (SVM, also support-vector network; Cortes & Vapnik 1995) is one of the most important supervised machine learning algorithms to be used for classification and regression. The regression algorithms of SVM, named support-vector regression (SVR), has been used in many astronomical studies, particularly in spectral data analysis (Liu et al. 2012, 2014, 2015a,b).

2.2. SLAM

SLAM has three hyper-parameters, two of which are penalty level (C) and tube radius (ϵ) coming from the genetic SVR algorithm. The third one (γ) indicates the width of the radial basis function (RBF), which is the kernel adopted by SLAM.

The architecture of SLAM consists of 3 steps:

1. **Pre-processing.** We normalize the spectra of the training data; in the mean time, we also standardize both stellar labels and spectral fluxes so that their mean is 0 and variance is 1;
2. **Training.** We train the SVR model with stellar parameters as independent variables and flux at given wavelength as dependent variable at each wavelength pixel using the training dataset;

3. Prediction. We apply the optimized SVR model to predict the stellar labels for observed spectra.

To choose the best-fit hyper-parameters at each wavelength, which is defined as training procedure, SLAM minimizes the k -fold cross-validated mean squared error (CV-MSE), which is defined as

$$MSE_j = \frac{1}{m} \sum_{i=1}^m [f_j(\vec{\theta}_i) - f_{i,j}]^2, \quad (1)$$

where $\vec{\theta}_i = (T_{eff,i}, \log g_i, [M/H]_i)$ denotes the stellar label vector of the i th star in the training data, $f_j(\vec{\theta}_i)$ is the j th pixel of the training spectra as a function of $\vec{\theta}_i$. In prediction procedure, the posterior probability density function of $\vec{\theta}$ for an observed spectrum can be written as

$$p(\vec{\theta}|f_{obs}) \propto p(\vec{\theta}) \prod_{j=1}^n p(f_{j,obs}|\vec{\theta}), \quad (2)$$

where $p(f_{j,obs}|\vec{\theta})$ is the likelihood of the spectral flux $f_{j,obs}$ varying with $\vec{\theta}$ based on the trained SVR model and $p(\vec{\theta})$ is the prior of $\vec{\theta}$. The best estimate of stellar labels can be found at the maximum of the posterior probability $p(\vec{\theta}|f_{obs})$. In practice, the logarithmic form of Eq. (2) as in below is used by adopting a Gaussian likelihood:

$$\begin{aligned} \ln p(\vec{\theta} | f_{obs}) = & -\frac{1}{2} \sum_{j=1}^n \frac{[f_{j,obs} - f_{j,model}(\vec{\theta})]^2}{\sigma_{j,obs}^2 + \sigma_{j,model}(\vec{\theta})^2} \\ & -\frac{1}{2} \sum_{j=1}^n \ln \left[2\pi \left(\sigma_{j,obs}^2 + \sigma_{j,model}(\vec{\theta})^2 \right) \right], \end{aligned} \quad (3)$$

where $f_{j,obs}$ is the j th pixel of the observed spectrum, $f_{j,model}(\vec{\theta})$ is the SVR model-predicted spectral flux corresponding to the stellar label vector $\vec{\theta}$. $\sigma_{j,obs}$ is the uncertainty of the j th pixel of the observed spectrum, and $\sigma_{j,model}(\vec{\theta})$ is the uncertainty of the j th pixel of the model-predicted spectrum given the stellar labels $\vec{\theta}$. In practice, $\sigma_{j,model}(\vec{\theta})$ is replaced with CV-MSE _{j} , which is independent of $\vec{\theta}$. SLAM adopts Maximum Likelihood Estimation (MLE) with Levenberg-Marquardt (LM, [Moré 1978](#)) least square optimizer as the optimization method to derive the most likely $\vec{\theta}$ for an observed spectrum.

3. DATA

3.1. LAMOST Data

LAMOST (Guo Shou Jing Telescope) is one of the most efficient spectroscopic survey telescopes providing 9,919,106 low-resolution ($R \sim 1800$) optical spectra, among which 8,966,416 are stellar spectra, in its sixth data release (DR6) ([Cui et al. 2012](#); [Deng et al. 2012](#); [Zhao et al. 2012](#)). 607,142 spectra are published as the M dwarf catalog in LAMOST DR6.

We firstly select stars from LAMOST DR6¹ M dwarf catalog ([Yi et al. 2014](#); [Guo et al. 2019](#)) cross-matched with *Gaia* DR2 ([Gaia Collaboration et al. 2018](#)). Then samples are selected using the

¹ <http://dr6.lamost.org>

following criteria to obtain both reliable *Gaia* photometry ($G_{BP} - G_{RP}$ color and G -band magnitude), astrometry (parallax) and LAMOST spectra.

1. `parallax / parallax_error > 5`;
2. `phot_bp_mean_flux/phot_bp_mean_flux_error > 20`,
`phot_rp_mean_flux/phot_rp_mean_flux_error > 20`,
 and `phot_g_mean_flux/phot_g_mean_flux_error > 20`;
3. `ruwe < 1.4`
4. signal-to-noise ratio (SNR) at i -band of LAMOST spectra is larger than 5.

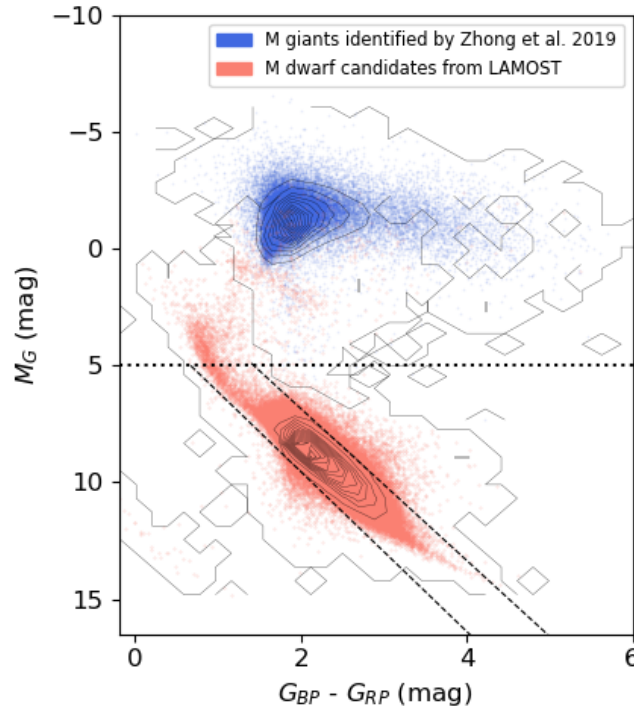


Figure 1. The panel shows the color-magnitude diagram, i.e. G -band absolute magnitude (M_G) versus $G_{BP} - G_{RP}$, of selected M dwarf samples compared with M giants from Zhong et al. (2019). The red stars represent the M dwarfs candidates from LAMOST survey, while the blue stars denote the M giants samples from Zhong et al. (2019). The horizontal dotted line represents the M_G equals to 5. The coordinates of the selected quadrangles enclosed by the dotted line and two dashed lines are [(0.7, 5), (1.4, 5), (4, 16.5), (5, 16.5)].

The criteria 1-3 aim to select stars with both accurate photometry and astrometry. `ruwe` is the re-normalised unit-weight error which measures astrometric goodness-of-fit, criteria 3 is to select stars with small re-normalised unit-weight error. Criteria 4 aims to select spectra with clear stellar spectral signature. Similar to B20, criteria 5 aims to select the main-sequence M dwarfs as shown in Fig. 1.

We display the selected M dwarf samples in H-R diagrams (Fig. 1). The G -band absolute magnitude is estimated from the Bayesian distance from Bailer-Jones et al. (2018). To investigate the

contamination of M giant stars, we draw 35,382 M giants on Fig. 1 (Zhong et al. 2019). We select $M_G + A_G \leq 5$ to remove the contaminations. Some of the M dwarf stars are not located at the main-sequence, but below and above the main-sequence. There are $\sim 7,000$ stars on the top side of the quadrangle which are likely pre-main sequence stars or binaries. And about 1,000 stars on the bottom side might be white dwarfs - MS binaries. We remove these stars and only select 379,258 M dwarf samples fell into the quadrangle for the estimation of the stellar parameters. Most of M dwarf stars are located within a few hundreds pc. Therefore, the interstellar extinction of M dwarfs are mostly very low. There may be a few stars with large extinction and thus location beyond the selection area. These stars may be removed mistakenly.

3.2. Training Dataset

Since SLAM is a data-driven model, which assumes stellar labels as ground truth, reliable stellar parameters of training datasets are needed. To date, various methods and training datasets have been developed and introduced to measure labels (stellar parameters) for M dwarfs. In this work, we use APOGEE stellar parameters and BT-Settl synthetic spectra, respectively, as the training dataset separately described in the following two subsections 3.2.1 and 3.2.2.

3.2.1. APOGEE labels as training data

García Pérez et al. (2016) presented the ASPCAP, which fits observed near-infrared spectra to synthetic spectra made with the code FERRE (Allende Prieto et al. 2006). The measurement of T_{eff} for M dwarfs reach the precision of 100K between $3550 < T_{eff} < 4200$ K, the **mean** precision of ASPCAP metallicities is 0.18 dex between $-1.0 < [M/H] < 0.2$ (Schmidt et al. 2016). For APOGEE DR16, Jönsson et al. (2020) used the new MARCS stellar atmospheric models which is continuous from 3000 to 4000K for T_{eff} . The stellar parameters of DR16 enhance significantly for cool stars with $T_{eff} < 3500$ K, avoiding discontinuities in ASPCAP at 3500K. As for the metallicity of DR16, the comparison with six well-studied open clusters shows a faint difference of 0.004 dex (Donor et al. 2020; Jönsson et al. 2020).

We cross-match our selected M dwarfs APOGEE DR16 catalog² and obtain about 4,317 common stars with LAMOST spectra and APOGEE labels as training data. We further select 3,785 samples using the following criteria:

1. $2800 < T_{eff} < 4500$ K;
2. T_{eff} uncertainty smaller than 100K;
3. $-2 < [M/H] < 0.5$ dex;
4. $[M/H]$ uncertainty smaller than 0.1 dex;
5. $\log g > 4$ dex.

3.2.2. BT-Settl as training data

Another independent training dataset is BT-Settl spectra. Unlike the empirical spectra with APOGEE stellar labels, the BT-Settl model atmospheres and synthetic spectra (Allard et al. 2013)

² <https://www.sdss.org/dr16/irspec/aspcap/>

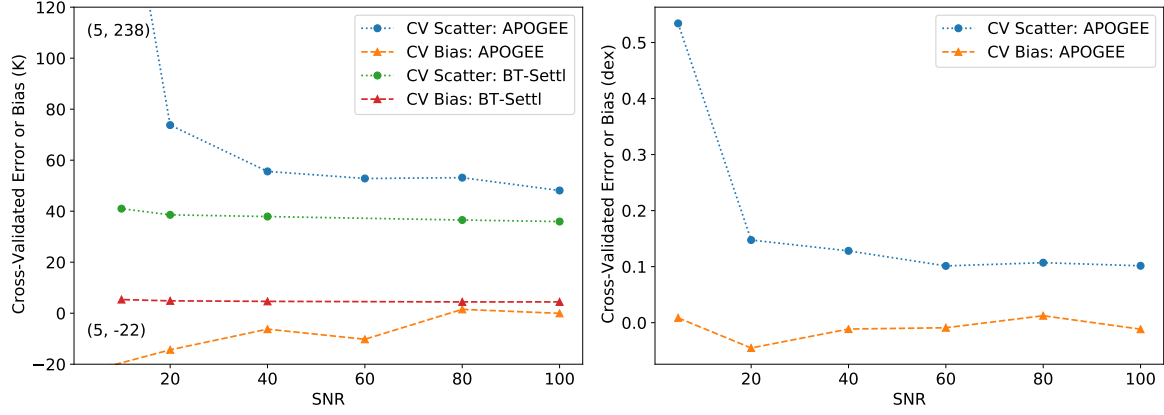


Figure 2. The figure displays how the cross-validation (CV) errors of stellar labels change with the signal-to-noise ratio (SNR). In both panels, the dotted lines represent the CV-scatter, while the dashed lines denote the CV-bias. Note that the SNR for APOGEE labeled LAMOST spectra is the SNR in the i -band (SNR_i), the SNR of the BT-Settl synthetic spectra is added artificially. Clearly, all of the CV errors decrease as the SNR increases. When $\text{SNR}_i > 100$, the typical CV-scatters of T_{eff} and $[\text{M}/\text{H}]$ are 50K, 0.10 dex for the ASPCAP labels, respectively. The typical CV-scatter for the BT-Settl labels is 40K when $\text{SNR} > 100$.

are computed by solving the radiative transfer using the Mixing Length Theory (Böhm-Vitense 1958). The BT-Settl model can be used to determine the parameters from moderately active very-low-mass stars (VLMs), brown dwarfs to planetary-mass objects. The BT-Settl model would be a useful supplement and extend the effective temperature lower than 3000K. Since a data-driven method is more difficult to be trained at the edge of training labels, we finally use T_{eff} range from 2200K to 7000K as the training labels.

4. RESULTS

Table 1. Notation of the names of the stellar parameter of LAMOST M dwarfs from different training dataset. The LAMOST spectra with APOGEE labels are used to estimate both the effective temperature and metallicities. BT-Settl synthesis spectra are used to only determine T_{eff} .

Training dataset	LAMOST spectra with ASPCAP labels	BT-Settl synthesis spectra
effective temperature	TEFF_AP	TEFF_BT
metallicity	M_H_AP	-

Note that APOGEE stellar parameters and BT-Settl depend on different atmospheric models and are not necessarily consistent with each other. Therefore, we use them as the training data independently and predict two sets of stellar labels based on the two dataset.

We use observed (LAMOST spectra with APOGEE labels) and synthesis spectra (BT-Settl), respectively, as the training dataset. The notation of stellar parameters (T_{eff} , $[\text{M}/\text{H}]$) of LAMOST M dwarfs are named by the different training datasets as shown in Table 1.

Firstly, we estimate the T_{eff} and $[\text{M}/\text{H}]$ using the APOGEE labels as the training set described in subsection 4.1.1 (T_{eff}) and 4.2 ($[\text{M}/\text{H}]$). We further use the synthetic spectra from BT-Settl models and obtain TEFF_BT. More details are discussed in subsection 4.1.2.

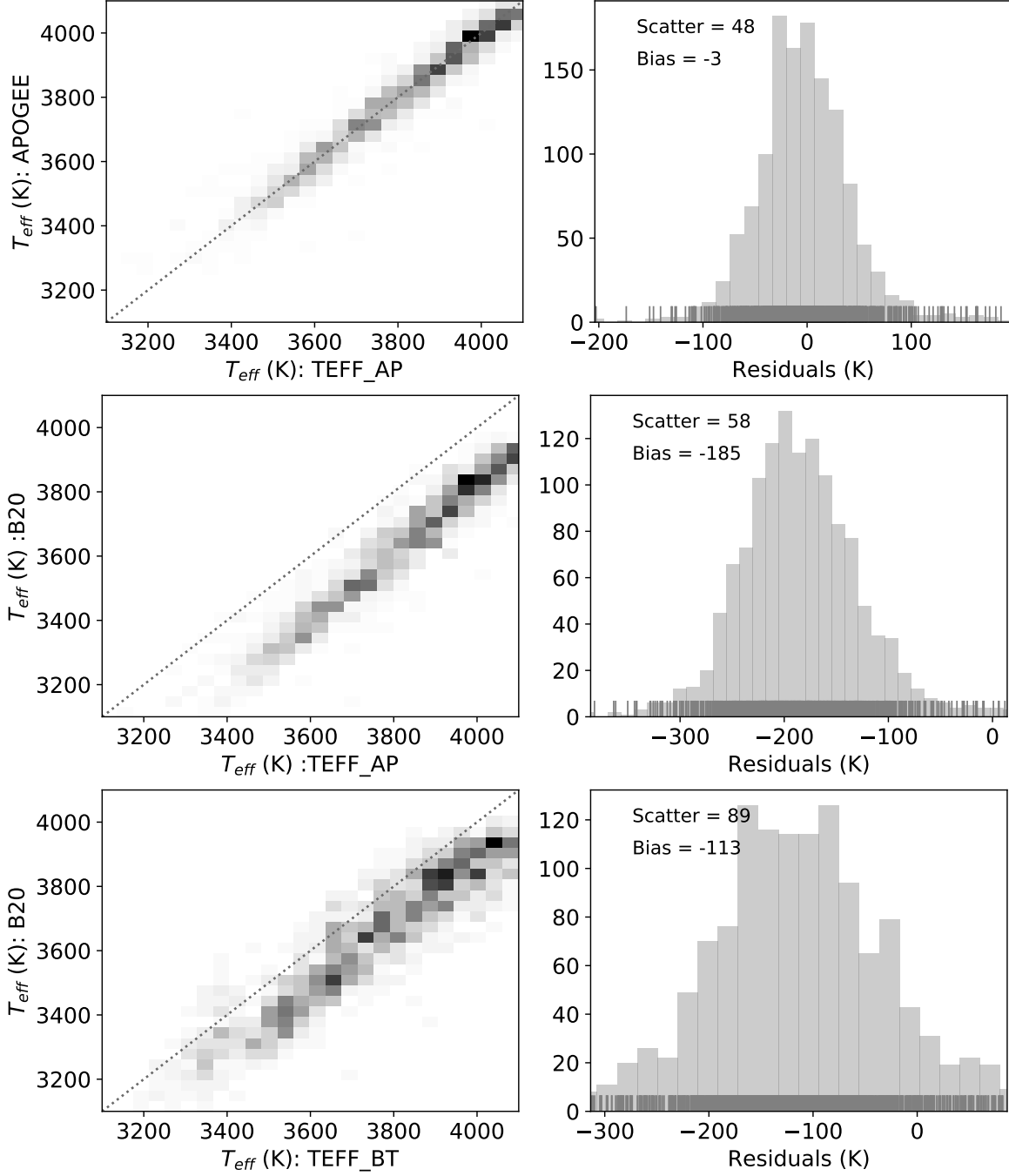


Figure 3. The top panels are comparisons of the ASPCAP-trained T_{eff} (TEFF_AP) and APOGEE stellar labels. The top-right panel shows the distribution of their residuals. While the middle panels show the comparison between TEFF_AP and B20. The bottom panels show the similar comparison, but between BT-Settl-trained T_{eff} (TEFF_BT) and B20.

4.1. Effective Temperature

4.1.1. APOGEE temperature

First of all, we combine the LAMOST spectra with the corresponding APOGEE labels as the training dataset to train the SLAM model. Effective temperature (TEFF_AP) and metallicity (M_H_AP)

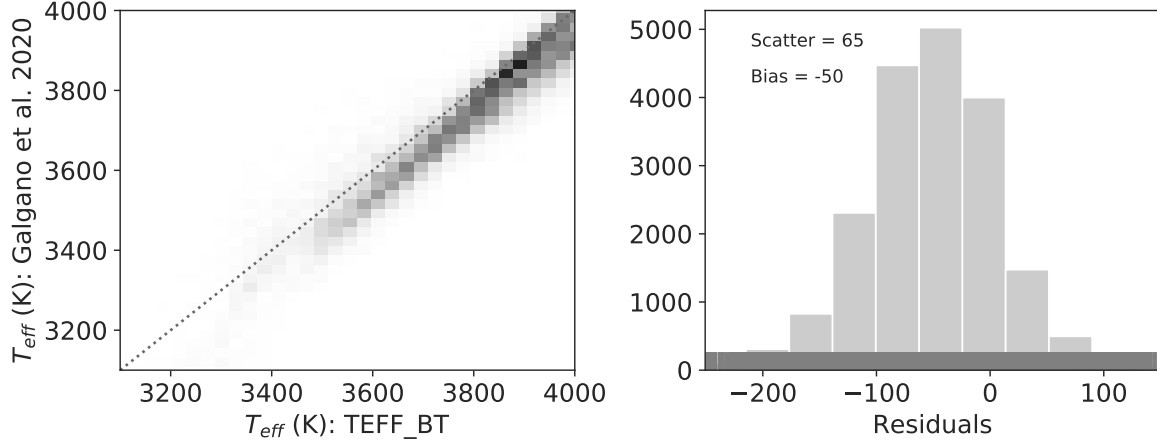


Figure 4. The left panel show the comparison between BT-Settl-trained T_{eff} (TEFF_BT) and Galgano et al. (2020). The right panel displays the distribution of the residuals.

are determined for the test dataset by applying this SLAM model. In this section, we discuss TEFF_AP and leave M_H_AP in subsection 4.2.

A 10-fold cross-validation (CV) is taken to estimate the precision and accuracy of the ASPCAP-trained SLAM labels. The CV-scatter and CV-bias denote the standard deviation and mean deviation respectively, and can be written as

$$\text{CV} - \text{bias} = \frac{1}{n} \sum_{i=1}^n (\theta_{i,SLAM} - \theta_i), \quad (4)$$

and

$$\text{CV} - \text{scatter} = \frac{1}{n} \sqrt{\sum_{i=1}^n (\theta_{i,SLAM} - \theta_i)^2}, \quad (5)$$

where $\theta_{i,SLAM}$ is the stellar label of the i th star predicted by SLAM. θ_i denotes the stellar label of the i th star as ground truth. Theoretically, a robust data-driven algorithm has a small CV bias and CV scatter. The CV results displayed in Fig. 2 indicate that the TEFF_AP reaches a precision of 50K with no bias when $\text{SNR}_i > 100$.

B20 derives spectroscopic temperatures and metallicities for 5,875 M dwarfs from the APOGEE survey. We cross-match the LAMOST data with their results and obtained 1,913 common stars. Among them, B20, LAMOST, and APOGEE DR16 together have 1,286 common stars. We compare the stellar parameters in the two catalogs separately with those we obtained using SLAM. As illustrated in the top-panel of Fig. 3, T_{eff} of APOGEE DR16 and TEFF_AP are in good agreement, which is not surprising because TEFF_AP are estimated by stellar labels of APOGEE. The ~ 50 K scatter and 3K bias are identical to the test results of CV, which are reasonable. The mid-panel of Fig. 3 shows the comparison between TEFF_AP and B20, the residuals between the two have a dispersion of ~ 60 K, and an offset of 185K. This bias is mainly due to the 182K difference between the temperature of APOGEE and B20. This is the result of different stellar atmospheric models used in the stellar parametrization.

4.1.2. BT-Settl temperature

We then set up the alternative training dataset using BT-Settl synthetic spectra so that the lower T_{eff} can go down beyond 3000K. We follow the preprocessing procedure developed by Zhang et al. (2020)³ to adjust the resolution and wavelength to be same as LAMOST low-resolution spectra. The training labels of the model grids⁴ are $2200 < T_{eff} < 7000\text{K}$, $-1.0 < [M/H] < 0.0$ dex, $2.5 < \log g < 5.5$ dex with steps of 100K, 0.5 dex and 0.5 dex, respectively.

The original grid from BT-Settl is too sparse. So we firstly interpolate the grid to obtain a new training dataset with denser grids. Because SLAM is a forward model, it can be used to do the interpolation. We randomly draw 15,000 points in the parameter space with $2800 < T_{eff} < 4500$ K, $-1.0 < [M/H] < 0.0$ dex and $4.5 < \log g < 5.5$ dex following the uniform distributions. And the corresponding synthetic spectra are obtained from the SLAM model *SLAM_0*, which is trained by the sparse original grid of BT-Settl. We then train model *SLAM_1* with the 15,000 synthetic spectra interpolated from model *SLAM_0* as training dataset. Finally, we predict TEFF_BT for the LAMOST spectra using *SLAM_1*.

Similar to subsection 4.1.1, 10-fold cross-validation is used to test the performance and robustness of our model. Random Gaussian noise is added to the test spectra. The left panel of Fig. 2 shows that CV errors change with a given signal-to-noise ratio (SNR). We obtain a random error of 40K with CV-bias of 5K at $\text{SNR} > 100$. The results of the CV errors indicate that our method effectively works. Fig. 2 also shows that CV-scatter varies with SNR. Note that the SNR is calculated by noise artificially added on fluxes of the normalized BT-Settl synthetic spectra.

We compare the temperatures with literature to assess the performance of our approach. Comparisons with B20 show that TEFF_BT are in agreement with their results with a scatter of $\sim 90\text{K}$ and an offset of $\sim 110\text{K}$ (see Fig. 3). Muirhead et al. (2018) presented *TESS* Cool Dwarf Catalog providing 1,140,255 cool dwarfs with T_{eff} determined on the basis of the empirical color-temperature relations of Mann et al. (2015). We cross-match LAMOST M dwarfs with this cool dwarf catalog and compare the stellar parameters. We find that TEFF_BT agrees with the *TESS* catalog with a scatter of 114K and an offset of $\sim 100\text{K}$. This is similar to the comparison with B20, which is not surprising since the T_{eff} of both B20 and *TESS* Cool Dwarf Catalog are calibrated with Mann et al. (2015). Finally, TEFF_BT is compared with Galgano et al. (2020), which estimate stellar parameters of $\sim 30,000$ M dwarfs from LAMOST DR1 based on *TESS* Cool Dwarf Catalog, as shown in Fig. 4. As expected, the residuals of T_{eff} in Fig. 4 demonstrate a small scatter of 65K and an offset of 50. Compared to other results, the smaller difference is due to the fact that both Galgano et al. (2020) and we used the same LAMOST spectra to estimate the effective temperatures.

4.2. Metallicity

Before estimating the metallicities of LAMOST M dwarfs, we first compared the $[M/H]$ of APOGEE DR16 and $[Fe/H]$ of B20, with a residual difference of only 0.1 dex, while B20 is overall more metal-rich than APOGEE by 0.2 dex. We find metallicity of APOGEE and B20 have better consistency where the metallicity abundance is higher. For stars with $[M/H]$ larger than -0.25, the scatter between B20 and APOGEE is 0.07 dex with an offset of 0.15 dex. While for stars with $[M/H] < -0.25$, the scatter and bias are 0.15 and 0.25 dex, respectively.

³ <https://github.com/hypergravity/astroslam>

⁴ <https://phoenix.ens-lyon.fr/Grids/BT-Settl/CIFIST2011b>

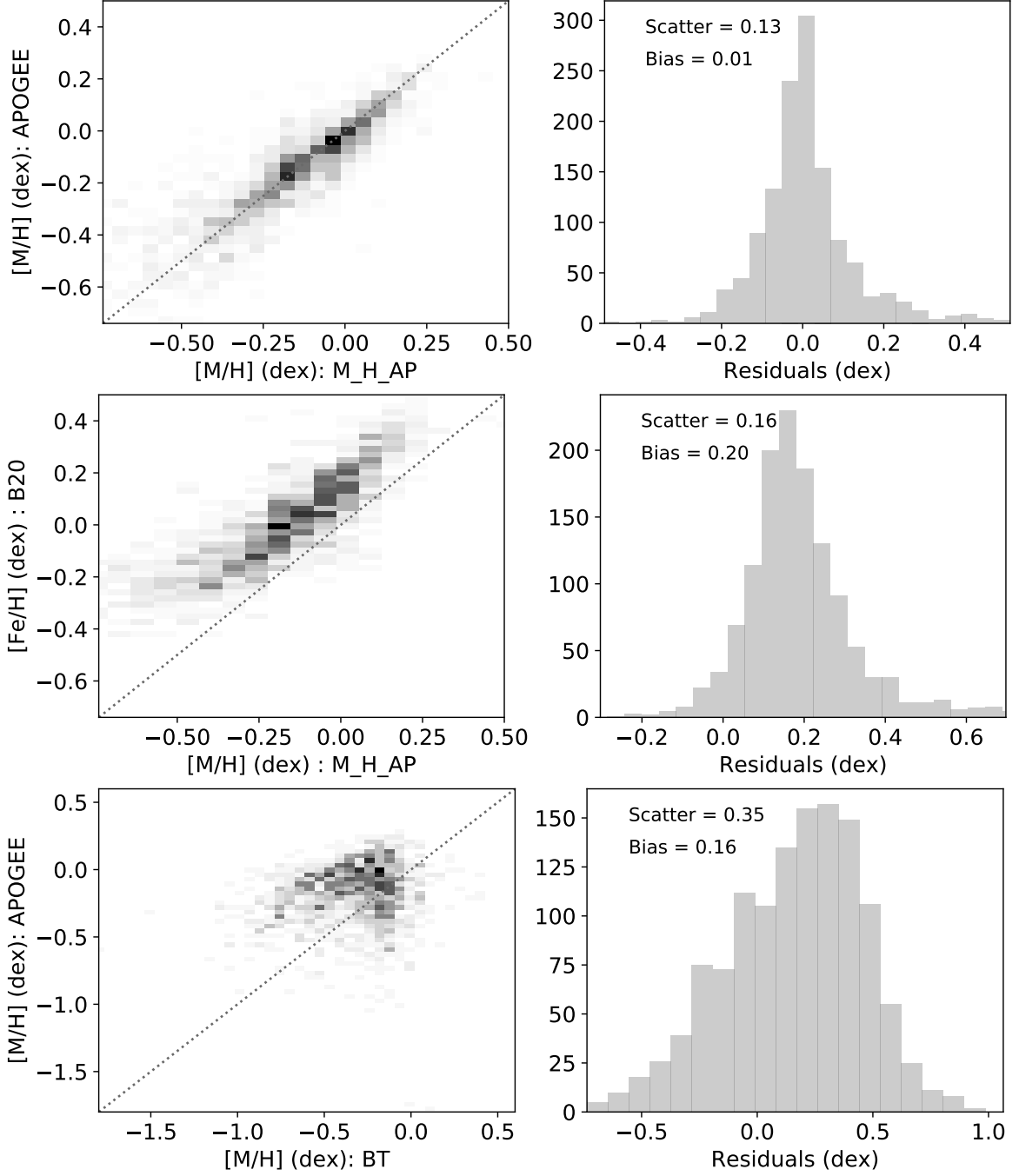


Figure 5. The top-left panel shows the comparison between APOGEE-trained $[M/H]$ (M_H_AP) and metallicities of APOGEE. The top-right panel displays the residuals of the metallicities with a scatter of 0.13 dex and no bias. The middle panels display the comparison between M_H_AP and B20. The residuals of M_H_AP and B20 shows a 0.16 dex scatter and a 0.2 dex bias. The bottom panel shows the comparison with metallicities derived by BT-Settl synthetic spectra and $[M/H]$ of APOGEE, they have a 0.35 dex scatter and a 0.16 dex offset.

M_H_AP is determined by $[M/H]$ of APOGEE as the training dataset. The prediction of M_H_AP is estimated at the same time as the TEFF_AP using SLAM. We find M_H_AP agrees well with APOGEE labels (see the top-panel of Fig. 5). Their good agreement is exactly what we expected,

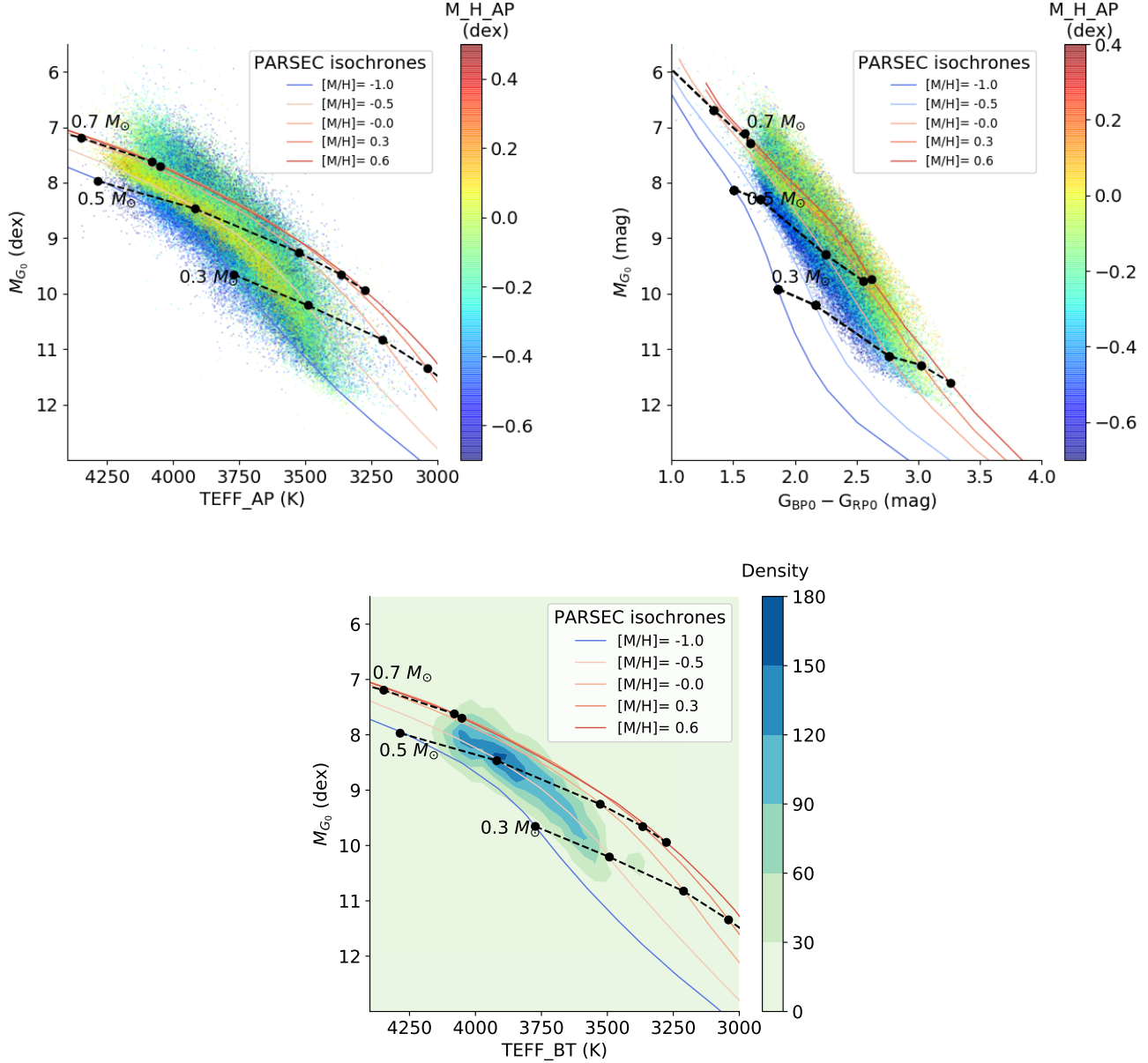


Figure 6. The top-left panel displays the HR-diagram of $\sim 9,000$ M dwarf stars with $SNR_i > 50$, a subsample of our catalog in the SLAM T_{eff} ($TEFF_AP$) versus *Gaia* M_G plane, and is colored by M_H_AP . The top-right panel shows the same HRD as the top-left panel, but the x-axis is $G_{BP} - G_{RP}$ colors. The bottom panel displays the contours drawn with the same stars as the left panel, while the temperatures are $TEFF_BT$. The solid lines indicate the PARSEC isochrones from $[M/H] = -1.0$ dex to $[M/H] = 0.6$ dex. The grey dashed curves represent the locations of 0.3 , 0.5 and $0.7 M_\odot$.

since the APOGEE parameters are used as the training labels. Furthermore, M_H_AP is in agreement with B20 metallicity with a scatter of 0.16 dex as shown in the mid-panel of Fig. 5. We also find a similar scenario to the comparison between APOGEE and B20. For stars with $[M/H] > -0.25$, the scatter is ~ 0.1 dex with a bias of 0.14 dex, but for stars with metallicities lower than -0.25 dex, the scatter is 0.2 dex with a 0.3 dex offset.

Metallicities could be also estimated by the BT-Settl models together with T_{eff} . However, the derived BT-Settl $[M/H]$ (hereafter, M_H_BT) shows no clear correlation with observed data published in previous studies (see the bottom-panel of Fig 5). In the metal-poor regime ($[M/H] < -0.25$ dex), though with larger scatter, the correlation between M_H_BT and APOGEE metallicities is obvious. But for $[M/H] > -0.25$ dex, M_H_BT is not able to distinguish well the metallicities of stars. This is probably due to the lack of model grids with $[M/H] > 0$. Therefore, the BT-Settl-trained $[M/H]$ is not adopted in our catalog Table 4.

4.3. *Hertzsprung-Russell Diagram*

Fig. 6 displays the Hertzsprung-Russell Diagram (HRD) of the LAMOST M dwarfs in the *Gaia* M_G versus logarithmic T_{eff} (TEFF_AP) plane. Note that the M_G is estimated from the Bayesian distance from Bailer-Jones et al. (2018) with extinction removed. 3D dust-reddening maps from *Bayestar* (Green et al. 2019) is used to estimate the visual extinction A_V for each star. A_G is further estimated from A_V using the extinction factor from Wang & Chen (2019). Fig. 6 is the de-reddened HRD for a sub-sample of $\sim 9,000$ M dwarf stars in our catalog. As illustrated in the top-left panel, the metallicity (M_H_AP) can be clearly distinguished in HRD. Moreover, the top-right panel shows the color-magnitude diagram in $G_{BP} - G_{RP}$ versus M_G plane, the gradient of metallicity is still very clear and shows the similar trend as in the top-left panel.

We further overlap the PARSEC (the Padova and Trieste Stellar Evolutionary Code) (Bressan et al. 2012) theoretical tracks with the age of 1 Gyr and find that they are well fit with each other as shown in the bottom panel of Fig. 6. The PARSEC version 1.2S⁵ (Chen et al. 2014) provides revisions on very-low-mass stars (VLMs) from the BT-Settl model with a wide range of metallicities from -2.19 to +0.70 dex. As displayed in Fig. 6, we found: a) The HRD given by the PARSEC stellar model shows good agreement with our observed HRD for TEFF_AP and TEFF_BT; b) Stars above the isochrone of $[M/H] = 0.6$ are likely to be in binary systems.

4.4. *Chromospheric Activity*

Considering active M dwarf is the only class of stars for which magnetic field affects overall stellar parameters systematically Kochukhov (2021). H α emission which can be the indicator of chromospheric activity might alter the reliability of the stellar parametrization. Guo et al. (2015) found that the fraction of active stars increases as spectral subtype becomes later. In our work, there is ~ 8 percent of M dwarf stars that have active magnetic fields. So during the procedure of data pre-processing, the pixels at the wavelength of H α emission are masked to improve the precision of stellar parameter estimation.

4.5. *The Catalog*

Table 2 shows the field definition of the stellar parameter catalog of our results. The important information of both the LAMOST and *Gaia* observations are presented in our catalog. TEFF_AP, TEFF_AP_ERR, M_H_AP and M_H_ERR are the ASPCAP-trained SLAM effective temperature and metallicity with the corresponding uncertainty. TEFF_BT and TEFF_BT_ERR are the BT-Settl-trained SLAM T_{eff} with the estimated uncertainty. Note that the *type* column is adopted from Guo et al. (2015), which indicates the magnetic activity determined by measuring H α activity. The

⁵ <http://stev.oapd.inaf.it/cgi-bin/cmd>

stellar parameters including T_{eff} and $[M/H]$ with the corresponding uncertainties of LAMOST M dwarfs estimated in this work are presented in Table 4.

5. DISCUSSION AND CONCLUSIONS

5.1. The accuracy of metallicity assessed from Open Clusters

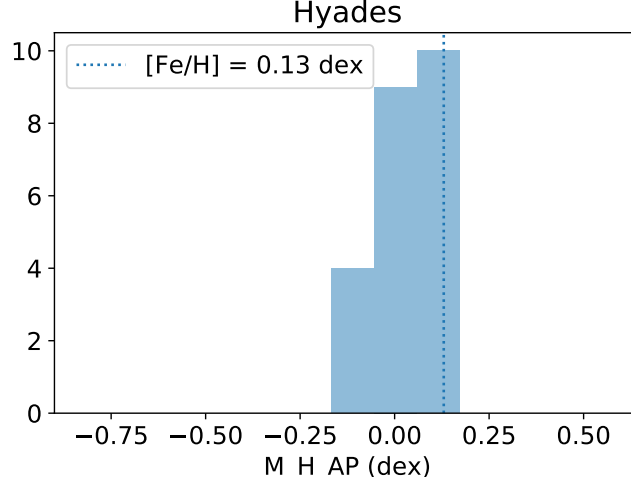


Figure 7. Metallicity distribution in Hyades. The vertical line indicate the metallicity $[Fe/H]=0.13$ given by previous studies.

Table 2. The field definition of the stellar parameters catalog of LAMOST M dwarf stars.

Column	Unit	Description
source_id		<i>Gaia</i> identification ID
obsid		LAMOST unique spectra ID
ra_obs	deg	LAMOST fiber pointing right ascension
dec_obs	deg	LAMOST fiber pointing declination
snru		LAMOST signal noise at SDSS <i>u</i> -band
snrg		LAMOST signal noise at SDSS <i>g</i> -band
snrr		LAMOST signal noise at SDSS <i>r</i> -band
snri		LAMOST signal noise at SDSS <i>i</i> -band
snrz		LAMOST signal noise at SDSS <i>z</i> -band
z		LAMOST redshift
z_err		LAMOST redshift uncertainty
type		magnetic activity
TEFF_BT	K	effective temperature from BT-Settl-trained SLAM
TEFF_BT_ERR	K	uncertainty of effective temperature from BT-Settl-trained SLAM
TEFF_AP	K	effective temperature from ASPCAP-trained SLAM
TEFF_AP_ERR	K	uncertainty of effective temperature from ASPCAP-trained SLAM
M_H_AP	dex	$[M/H]$ from ASPCAP-trained SLAM
M_H_AP_ERR	dex	uncertainty of $[M/H]$ from ASPCAP-trained SLAM

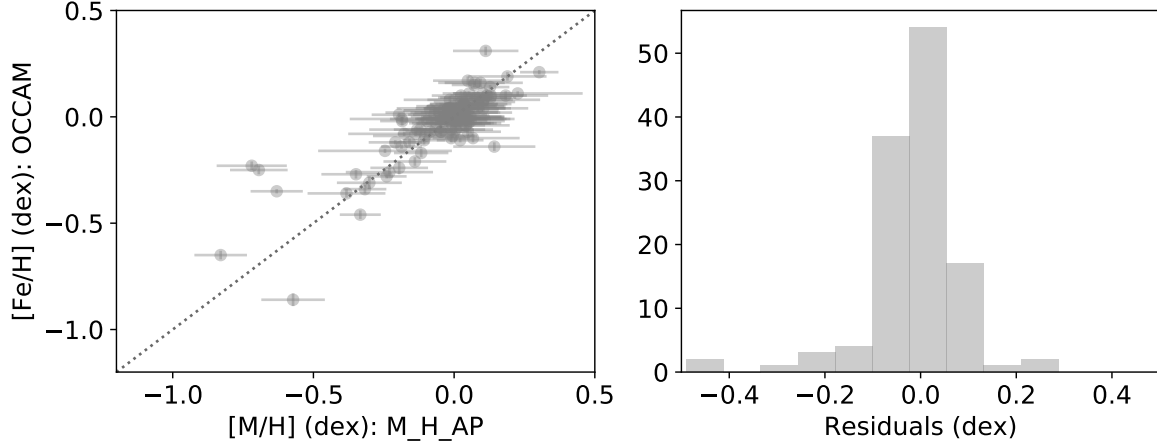


Figure 8. The left panel shows the comparison of M.H.AP and $[\text{Fe}/\text{H}]$ determined by Donor et al. (2020). The right panel displays the distribution of $[\text{M}/\text{H}]$ difference.

To assess the accuracy of the metallicities estimated in our work, we select 23 Hyades member stars from our catalog. Hyades is the nearest open cluster, as far as we know (van Leeuwen 2009), with a metallicity of about $+0.13$ dex (Schuler et al. 2006). We select all stars in a circle with a radius of 5 degrees, centered on right ascension of 66.725° and declination of 15.867° from *Gaia* DR2. Then, we adopt that stars located within $4 < \text{pmra} / \text{parallax} < 6$, $-2.5 < \text{pmdec} / \text{parallax} < 0$ and $0.04 < \text{parallax} < 0.05$, where *pmra* and *pmdec* are *Gaia* proper motions, are the member stars of Hyades. We cross-match our catalog with this sample and obtain 23 M dwarf member stars. We find

Table 3. The comparison of $[\text{M}/\text{H}]$ of LAMOST M dwarf stars with OCCAM. $\langle \text{M.H.AP} \rangle$ is the mean metallicity in each cluster derived by our work, $[\text{Fe}/\text{H}]_{\text{OCCAM}}$ is the mean value given by OCCAM and N is the number of the member in the cluster.

Cluster	$\langle \text{M.H.AP} \rangle$	$[\text{Fe}/\text{H}]_{\text{OCCAM}}$	N
ASCC 16	-0.07 ± 0.03	-0.04 ± 0.03	5
ASCC 21	-0.21 ± 0.03	-0.12 ± 0.04	2
Berkeley 19	-0.19	-0.01	1
Berkeley 29	0.08	0.09	1
Briceno 1	-0.06	-0.03	1
Chupina 1	-0.63	-0.35	1
Chupina 3	-0.11	-0.11	1
Chupina 5	-0.83	-0.65	1
Collinder 69	-0.20 ± 0.08	-0.21 ± 0.14	5
Collinder 70	0.01	-0.01	1
Koposov 62	-0.05	0.07	1
Melotte 20	0.05 ± 0.11	0.05 ± 0.12	21
Melotte 22	0.00 ± 0.13	0.00 ± 0.09	66
NGC 2420	-0.23	-0.26	1
NGC 2682	-0.16 ± 0.25	-0.22 ± 0.30	7
NGC 752	-0.17 ± 0.26	-0.09 ± 0.11	6

that the distribution of M_H_AP of the members has a mean of 0.0 dex and a standard deviation of 0.1 dex, as shown in Fig. 7. This result tentatively verifies that the accuracy of M_H_AP is around 0.1 dex.

Furthermore, we cross-match our catalog with the Open Cluster Chemical Analysis and Mapping (OCCAM) survey (Donor et al. 2020) and obtain 138 member stars belonging to 15 open clusters. Fig. 8 compares $[Fe/H]$ given by Donor et al. (2020) with M_H_AP . The left panel shows that M_H_AP matches very well with the metallicity of the corresponding clusters in the ranges from -0.7 to 0.4 dex. A few stars with higher metallicity in literature are estimated as lower metallicity using our method. This may implies some limit of the estimation in metal-poor regime. The right panel of Fig. 8 displays the distribution of residuals between M_H_AP and $[Fe/H]$ of OCCAM. The mean value is 0.01 dex and the standard deviation is 0.1 dex. This illustrates that the uncertainty of the metallicity derived in this work is around 0.1 dex. Detailed information on the comparison of metallicities of cluster members is shown in Table. 3.

5.2. Precision of metallicity from wide binary

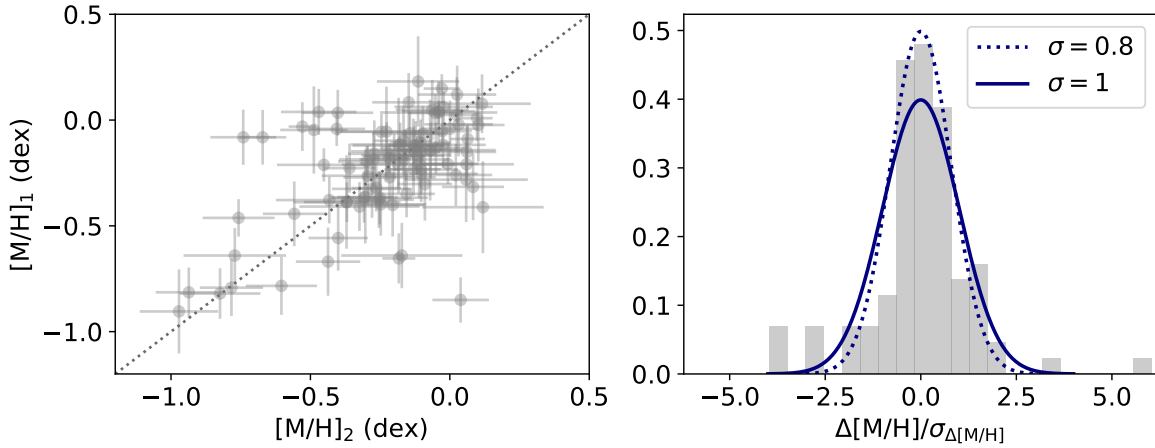


Figure 9. Comparison of metallicities of high-confidence binaries with separations less than 3,000 au. Left: comparison of the metallicities (M_H_AP) of the primary and secondary component. Right: distributions of uncertainty-normalized $[M/H]$ difference, compared to Gaussians with the corresponding σ .

We further assess the precision of the metallicity using M dwarf - M dwarf wide binaries (Qiu et al., in prep). We start with the catalog of initial wide binaries candidates released by Tian et al. (2020), which contains 807,611 candidates, selected from *Gaia* DR2 within a distance of 4.0 kpc and a maximum projected separation $s = 1.0$ pc. This catalog contains many types of wide binaries (e.g., main sequence - main sequence, main sequence - white dwarf, white dwarf - white dwarf etc.), and these wide binary stars may be polluted by visual binaries (chance alignments) at large separations, as described in Section 3.5 in Tian et al. (2020). We finally choose 92 pairs of binary stars with the separations less than 3,000 au to assess the precision of $[M/H]$.

Fig. 9 compares the differences of the metallicities (M_H_AP) of the companions of these binaries. M_H_AP is expected to be consistent with each other if the companions are physically associated. The left panel shows the pairs have similar $[M/H]$, only 2 of the 92 systems fall outside of 3-sigma range. These outliers are most likely not physical binary stars. The mean difference of metallicity of the primary and secondary companions is 0.01 dex with scatter of 0.23

dex. The right panel is the uncertainty-normalized metallicity difference; i.e., $\Delta[M/H]/\sigma_{\Delta[M/H]} = ([M/H]_1 - [M/H]_2)/\sqrt{\sigma_{[M/H]_1}^2 + \sigma_{[M/H]_2}^2}$. If the derived $\sigma_{[M/H]}$ values are accurate, the uncertainty-normalized metallicity difference should be distributed as a Gaussian distribution with $\sigma = 1$. As shown in the right panel, the distribution matches better with $\sigma \sim 0.8$, which suggests that M_H_AP uncertainties may be overestimated by $\sim 20\%$.

5.3. Summary

In this work, we have derived a spectroscopic catalog of stellar parameters for $\sim 300,000$ M dwarf stars. Precise effective temperatures and metallicities of M dwarf stars from LAMOST DR6 and *Gaia* DR2 with are given in this catalog. Stars located within the range of $2800 < T_{eff} < 4500\text{K}$ (both of TEFF_AP and TEFF_BT) are finally adopted in our catalog. Two versions of effective temperatures are obtained with precisions of 40K for TEFF_BT and 50K for TEFF_AP at SNR > 50 . Particularly, TEFF_AP agrees with B20 with a 60K scatter and a 185K offset. The systematic errors come from different stellar atmospheric models, in this case, BT-Settl model and MARCS, respectively.

This study provides a method using BT-Settl model to obtain the parameters of LAMOST M dwarf stars. We also publish the code and the stellar parametrization pipeline on the website⁶. Note that the data-driven method to derive stellar labels strongly relies on training datasets, for the estimation in this work is on BT-Settl model and stellar parameters of APOGEE. We address that SLAM can be used as the industrial framework against which to decode the stellar parameters of the cool atmosphere of M dwarf stars in the upcoming surveys such as SDSS-V (Kollmeier et al. 2017).

ACKNOWLEDGMENTS

We thank the anonymous referee for the very helpful comments. This work is supported by National Key R&D Program of China No. 2019YFA0405500. C.L. thanks the National Natural Science Foundation of China (NSFC) with grant No. 11835057. Guoshoujing Telescope (the Large Sky Area Multi-Object Fiber Spectroscopic Telescope LAMOST) is a National Major Scientific Project built by the Chinese Academy of Sciences. Funding for the project has been provided by the National Development and Reform Commission. LAMOST is operated and managed by the National Astronomical Observatories, Chinese Academy of Sciences. This work has made use of data from the European Space Agency (ESA) mission *Gaia* (<https://www.cosmos.esa.int/gaia>), processed by the *Gaia* Data Processing and Analysis Consortium (DPAC, <https://www.cosmos.esa.int/web/gaia/dpac/consortium>). Funding for the DPAC has been provided by national institutions, in particular the institutions participating in the *Gaia* Multilateral Agreement.

Facilities: LAMOST, *Gaia*

Software: astropy (Astropy Collaboration et al. 2018), scipy (Virtanen et al. 2019), scikit-learn (Pedregosa et al. 2011), SLAM (Zhang et al. 2020), TOPCAT (Taylor 2005)

APPENDIX

⁶ <https://github.com/jiadonglee/MDwarfMachine>

Table 4. The stellar parameters (T_{eff} , [M/H]) of the LAMOST M dwarfs catalog. The complete table can be found online <http://paperdata.china-vo.org/jordan/Mdwarf/jdli21.fits>.

obsid	TEFF_BT	TEFF_BT_ERR	TEFF_AP	TEFF_AP_ERR	M_H_AP	M_H_AP_ERR	snri
300208242	3599	38	3804	66	0.14	0.16	46
331715172	3676	38	3746	73	-0.17	0.17	39
438102143	3587	36	3602	51	-0.21	0.12	74
285016161	3628	38	3612	76	-1.12	0.18	36
185605033	3680	38	3763	77	-0.23	0.18	35
400108239	3681	36	3749	49	-0.15	0.12	78
8003208	3584	38	3704	72	-0.25	0.17	40
364813026	3645	38	3777	85	0.03	0.20	29
387207221	3522	36	3612	47	-0.14	0.12	86
574612100	3451	38	3425	97	-0.52	0.22	23
21803121	3602	38	3692	76	-0.14	0.18	36
196704044	3606	38	3680	59	-0.20	0.14	57
212806086	3545	36	3669	48	0.09	0.12	82
593209154	3635	36	3724	45	-0.08	0.11	92
600415191	3645	36	3726	35	-0.18	0.09	144
333012162	3280	38	3472	92	-0.18	0.21	25
287010071	3380	38	3649	81	0.06	0.19	32
334502112	3643	38	3677	67	-0.38	0.16	45
353612149	3384	38	3474	63	-0.39	0.15	51
33107013	3507	36	3577	43	-0.10	0.11	100
557905051	3618	38	3626	60	-0.15	0.14	55

A. CATALOG

REFERENCES

- Allard, F., Homeier, D., Freytag, B., et al. 2013, *Memorie della Societa Astronomica Italiana Supplementi*, 24, 128.
<https://arxiv.org/abs/1302.6559>
- Allende Prieto, C., Beers, T. C., Wilhelm, R., et al. 2006, *ApJ*, 636, 804, doi: [10.1086/498131](https://doi.org/10.1086/498131)
- Astropy Collaboration, Price-Whelan, A. M., Sipőcz, B. M., et al. 2018, *AJ*, 156, 123, doi: [10.3847/1538-3881/aabc4f](https://doi.org/10.3847/1538-3881/aabc4f)
- Bailer-Jones, C. A. L., Rybizki, J., Foesneau, M., Mantelet, G., & Andrae, R. 2018, *AJ*, 156, 58, doi: [10.3847/1538-3881/aacb21](https://doi.org/10.3847/1538-3881/aacb21)
- Birky, J., Hogg, D. W., Mann, A. W., & Burgasser, A. 2020, *ApJ*, 892, 31, doi: [10.3847/1538-4357/ab7004](https://doi.org/10.3847/1538-4357/ab7004)
- Bochanski, J. J., Hawley, S. L., Covey, K. R., et al. 2010, *AJ*, 139, 2679, doi: [10.1088/0004-6256/139/6/2679](https://doi.org/10.1088/0004-6256/139/6/2679)
- Boeshaar, P. C. 1976, PhD thesis, Ohio State University, Columbus.
- Boeshaar, P. C., & Tyson, J. A. 1985, *AJ*, 90, 817, doi: [10.1086/113791](https://doi.org/10.1086/113791)
- Böhm-Vitense, E. 1958, *ZA*, 46, 108
- Boyajian, T. S., von Braun, K., van Belle, G., et al. 2012, *ApJ*, 757, 112, doi: [10.1088/0004-637X/757/2/112](https://doi.org/10.1088/0004-637X/757/2/112)

- Bressan, A., Marigo, P., Girardi, L., et al. 2012, *MNRAS*, 427, 127, doi: [10.1111/j.1365-2966.2012.21948.x](https://doi.org/10.1111/j.1365-2966.2012.21948.x)
- Chen, Y., Girardi, L., Bressan, A., et al. 2014, *MNRAS*, 444, 2525, doi: [10.1093/mnras/stu1605](https://doi.org/10.1093/mnras/stu1605)
- Cortes, C., & Vapnik, V. 1995, *Machine learning*, 20, 273
- Covey, K. R., Hawley, S. L., Bochanski, J. J., et al. 2008, *AJ*, 136, 1778, doi: [10.1088/0004-6256/136/5/1778](https://doi.org/10.1088/0004-6256/136/5/1778)
- Cui, X.-Q., Zhao, Y.-H., Chu, Y.-Q., et al. 2012, *Research in Astronomy and Astrophysics*, 12, 1197, doi: [10.1088/1674-4527/12/9/003](https://doi.org/10.1088/1674-4527/12/9/003)
- Deng, L.-C., Newberg, H. J., Liu, C., et al. 2012, *Research in Astronomy and Astrophysics*, 12, 735, doi: [10.1088/1674-4527/12/7/003](https://doi.org/10.1088/1674-4527/12/7/003)
- Dieterich, S. B., Simler, A., Henry, T. J., & Jao, W.-C. 2020, arXiv e-prints, arXiv:2012.00915. <https://arxiv.org/abs/2012.00915>
- Donor, J., Frinchaboy, P. M., Cunha, K., et al. 2020, *AJ*, 159, 199, doi: [10.3847/1538-3881/ab77bc](https://doi.org/10.3847/1538-3881/ab77bc)
- Gaia Collaboration, Babusiaux, C., van Leeuwen, F., et al. 2018, *A&A*, 616, A10, doi: [10.1051/0004-6361/201832843](https://doi.org/10.1051/0004-6361/201832843)
- Galgano, B., Stassun, K., & Rojas-Ayala, B. 2020, *AJ*, 159, 193, doi: [10.3847/1538-3881/ab7f37](https://doi.org/10.3847/1538-3881/ab7f37)
- García Pérez, A. E., Allende Prieto, C., Holtzman, J. A., et al. 2016, *AJ*, 151, 144, doi: [10.3847/0004-6256/151/6/144](https://doi.org/10.3847/0004-6256/151/6/144)
- Green, G. M., Schlafly, E., Zucker, C., Speagle, J. S., & Finkbeiner, D. 2019, *ApJ*, 887, 93, doi: [10.3847/1538-4357/ab5362](https://doi.org/10.3847/1538-4357/ab5362)
- Guo, Y.-X., Yi, Z.-P., Luo, A. L., et al. 2015, *Research in Astronomy and Astrophysics*, 15, 1182, doi: [10.1088/1674-4527/15/8/007](https://doi.org/10.1088/1674-4527/15/8/007)
- Guo, Y. X., Luo, A. L., Zhang, S., et al. 2019, *MNRAS*, 485, 2167, doi: [10.1093/mnras/stz458](https://doi.org/10.1093/mnras/stz458)
- Ho, A. Y. Q., Ness, M. K., Hogg, D. W., et al. 2017, *ApJ*, 836, 5, doi: [10.3847/1538-4357/836/1/5](https://doi.org/10.3847/1538-4357/836/1/5)
- Jofré, P., Heiter, U., & Soubiran, C. 2019, *ARA&A*, 57, 571, doi: [10.1146/annurev-astro-091918-104509](https://doi.org/10.1146/annurev-astro-091918-104509)
- Jönsson, H., Holtzman, J. A., Allende Prieto, C., et al. 2020, *AJ*, 160, 120, doi: [10.3847/1538-3881/aba592](https://doi.org/10.3847/1538-3881/aba592)
- Kirkpatrick, J. D. 1992, PhD thesis, Arizona Univ., Tucson.
- Kirkpatrick, J. D., Reid, I. N., Liebert, J., et al. 1999, *ApJ*, 519, 802, doi: [10.1086/307414](https://doi.org/10.1086/307414)
- Kochukhov, O. 2021, *A&A Rv*, 29, 1, doi: [10.1007/s00159-020-00130-3](https://doi.org/10.1007/s00159-020-00130-3)
- Kollmeier, J. A., Zasowski, G., Rix, H.-W., et al. 2017, arXiv e-prints, arXiv:1711.03234. <https://arxiv.org/abs/1711.03234>
- Liu, C., Bailer-Jones, C. A. L., Sordo, R., et al. 2012, *MNRAS*, 426, 2463, doi: [10.1111/j.1365-2966.2012.21797.x](https://doi.org/10.1111/j.1365-2966.2012.21797.x)
- Liu, C., Deng, L.-C., Carlin, J. L., et al. 2014, *ApJ*, 790, 110, doi: [10.1088/0004-637X/790/2/110](https://doi.org/10.1088/0004-637X/790/2/110)
- Liu, C., Fang, M., Wu, Y., et al. 2015a, *ApJ*, 807, 4, doi: [10.1088/0004-637X/807/1/4](https://doi.org/10.1088/0004-637X/807/1/4)
- Liu, C., Cui, W.-Y., Zhang, B., et al. 2015b, *Research in Astronomy and Astrophysics*, 15, 1137, doi: [10.1088/1674-4527/15/8/004](https://doi.org/10.1088/1674-4527/15/8/004)
- Majewski, S. R., Schiavon, R. P., Frinchaboy, P. M., et al. 2017, *AJ*, 154, 94, doi: [10.3847/1538-3881/aa784d](https://doi.org/10.3847/1538-3881/aa784d)
- Mann, A. W., Feiden, G. A., Gaidos, E., Boyajian, T., & von Braun, K. 2015, *ApJ*, 804, 64, doi: [10.1088/0004-637X/804/1/64](https://doi.org/10.1088/0004-637X/804/1/64)
- Mann, A. W., Gaidos, E., & Ansdell, M. 2013, *ApJ*, 779, 188, doi: [10.1088/0004-637X/779/2/188](https://doi.org/10.1088/0004-637X/779/2/188)
- Mann, A. W., Dupuy, T., Kraus, A. L., et al. 2019, *ApJ*, 871, 63, doi: [10.3847/1538-4357/aaf3bc](https://doi.org/10.3847/1538-4357/aaf3bc)
- Moré, J. J. 1978, *The Levenberg-Marquardt algorithm: Implementation and theory*, Vol. 630, 105–116, doi: [10.1007/BFb0067700](https://doi.org/10.1007/BFb0067700)
- Muirhead, P. S., Dressing, C. D., Mann, A. W., et al. 2018, *AJ*, 155, 180, doi: [10.3847/1538-3881/aab710](https://doi.org/10.3847/1538-3881/aab710)
- Ness, M., Hogg, D. W., Rix, H. W., Ho, A. Y. Q., & Zasowski, G. 2015, *ApJ*, 808, 16, doi: [10.1088/0004-637X/808/1/16](https://doi.org/10.1088/0004-637X/808/1/16)
- Pedregosa, F., Varoquaux, G., Gramfort, A., et al. 2011, *Journal of Machine Learning Research*, 12, 2825
- Rajpurohit, A. S., Allard, F., Rajpurohit, S., et al. 2018, *A&A*, 620, A180, doi: [10.1051/0004-6361/201833500](https://doi.org/10.1051/0004-6361/201833500)
- Rajpurohit, A. S., Reylé, C., Allard, F., et al. 2014, *A&A*, 564, A90, doi: [10.1051/0004-6361/201322881](https://doi.org/10.1051/0004-6361/201322881)

- Schmidt, S. J., Wagoner, E. L., Johnson, J. A., et al. 2016, *MNRAS*, 460, 2611, doi: [10.1093/mnras/stw1139](https://doi.org/10.1093/mnras/stw1139)
- Schuler, S. C., Hatzes, A. P., King, J. R., Kürster, M., & The, L.-S. 2006, *AJ*, 131, 1057, doi: [10.1086/499103](https://doi.org/10.1086/499103)
- Skrutskie, M. F., Cutri, R. M., Stiening, R., et al. 2006, *AJ*, 131, 1163, doi: [10.1086/498708](https://doi.org/10.1086/498708)
- Taylor, M. B. 2005, in *Astronomical Society of the Pacific Conference Series*, Vol. 347, *Astronomical Data Analysis Software and Systems XIV*, ed. P. Shopbell, M. Britton, & R. Ebert, 29
- Tian, H.-J., El-Badry, K., Rix, H.-W., & Gould, A. 2020, *ApJS*, 246, 4, doi: [10.3847/1538-4365/ab54c4](https://doi.org/10.3847/1538-4365/ab54c4)
- Ting, Y.-S., Conroy, C., Rix, H.-W., & Cargile, P. 2019, *ApJ*, 879, 69, doi: [10.3847/1538-4357/ab2331](https://doi.org/10.3847/1538-4357/ab2331)
- Trifonov, T., Kürster, M., Zechmeister, M., et al. 2018, *A&A*, 609, A117, doi: [10.1051/0004-6361/201731442](https://doi.org/10.1051/0004-6361/201731442)
- van Leeuwen, F. 2009, *A&A*, 497, 209, doi: [10.1051/0004-6361/200811382](https://doi.org/10.1051/0004-6361/200811382)
- Vapnik, V., Golowich, S. E., & Smola, A. J. 1997, 281
- Veyette, M. J., Muirhead, P. S., Mann, A. W., et al. 2017, *ApJ*, 851, 26, doi: [10.3847/1538-4357/aa96aa](https://doi.org/10.3847/1538-4357/aa96aa)
- Virtanen, P., Gommers, R., Oliphant, T. E., et al. 2019, arXiv e-prints, arXiv:1907.10121. <https://arxiv.org/abs/1907.10121>
- Wang, S., & Chen, X. 2019, *ApJ*, 877, 116, doi: [10.3847/1538-4357/ab1c61](https://doi.org/10.3847/1538-4357/ab1c61)
- Wolf, V. M., & Wallerstein, G. 2005, *MNRAS*, 356, 963, doi: [10.1111/j.1365-2966.2004.08515.x](https://doi.org/10.1111/j.1365-2966.2004.08515.x)
- Xiang, M., Ting, Y.-S., Rix, H.-W., et al. 2019, *ApJS*, 245, 34, doi: [10.3847/1538-4365/ab5364](https://doi.org/10.3847/1538-4365/ab5364)
- Yi, Z., Luo, A., Song, Y., et al. 2014, *AJ*, 147, 33, doi: [10.1088/0004-6256/147/2/33](https://doi.org/10.1088/0004-6256/147/2/33)
- Zhang, B., Liu, C., & Deng, L.-C. 2020, *ApJS*, 246, 9, doi: [10.3847/1538-4365/ab55ef](https://doi.org/10.3847/1538-4365/ab55ef)
- Zhao, G., Zhao, Y.-H., Chu, Y.-Q., Jing, Y.-P., & Deng, L.-C. 2012, *Research in Astronomy and Astrophysics*, 12, 723, doi: [10.1088/1674-4527/12/7/002](https://doi.org/10.1088/1674-4527/12/7/002)
- Zhong, J., Li, J., Carlin, J. L., et al. 2019, *ApJS*, 244, 8, doi: [10.3847/1538-4365/ab3859](https://doi.org/10.3847/1538-4365/ab3859)